Semi-inclusive deep-inelastic scattering off few-nucleon systems: Tagging the EMC effect and hadronization mechanisms with detection of slow recoiling nuclei

C. Ciofi degli Atti and L. P. Kaptari[*]

Department of Physics, University of Perugia, Piazza dell' Università 1, I-06123 Perugia, Italy and
Istituto Nazionale di Fisica Nucleare, Sezione di Perugia, Via A. Pascoli, I-06123 Perugia, Italy

The semi-inclusive deep-inelastic scattering of electrons off ^{2}H and ^{3}He with detection of slow protons and deuterons, respectively, i.e., the processes ^{2}H$(e, e'p)X$ and ^{3}He$(e, e'd)X$, are calculated within the spectator mechanism, taking into account the final state interaction of the nucleon debris with the detected protons and deuterons. It is shown that by a proper choice of the kinematics the origin of the EMC effect and the details of the interaction between the hadronizing quark and the nuclear medium can be investigated at a level which cannot be reached by inclusive deep-inelastic scattering. A comparison of the results of our calculations, containing no adjustable parameters, with recently available experimental data on the process ^{2}H$(e, e'p)X$ shows a good agreement in the backward hemisphere of the emitted nucleons. Theoretical predictions at energies that will be available at the upgraded Thomas Jefferson National Accelerator Facility are presented, and the possibility to investigate the proposed semi-inclusive processes at electron-ion colliders is briefly discussed.

I. INTRODUCTION

In spite of many experimental and theoretical efforts (for a recent review, see Ref. [1]), the origin of the nuclear EMC effect has not yet been fully clarified, and the problem as to whether the quark distribution of nucleons undergoes deformations due to the nuclear medium remains open. Understanding the origin of the EMC effect would be of great relevance in many respects; consider, for example, that most QCD sum rules and predictions require the knowledge of the neutron quark distributions, which can only be extracted from nuclear experiments; this implies, from one side, a reliable knowledge of various nontrivial nuclear properties such as the nucleon removal energy and momentum distributions and, from the other side, a proper treatment of the lepton-nucleus reaction mechanism, including the effect of the final state interaction (FSI) of the leptoproduced hadrons with the nuclear medium. Since the dependence of the EMC effect upon the momentum transfer Q^2 and the Bjorken scaling variable x_{Bj} is smooth, the measurements of the nuclear quark distributions in inclusive deep-inelastic scattering (DIS) processes have not yet determined enough constraints to distinguish between different theoretical approaches. To progress in this field, one should go beyond inclusive experiments, e.g., by considering semi-inclusive deep-inelastic scattering (SIDIS) processes in which another particle is detected in coincidence with the scattered electron. The "classical" SIDIS processes are the ones in which a fast hadron, arising from the leading quark hadronization, is detected in coincidence with the scattered electron. This type of SIDIS has provided much information on hadronization in the medium (for a recent review, see Ref. [2]), but not on the EMC effect. An alternative type of SIDIS, namely, the one in which,

instead of the high-energy leading hadron, a nucleus $(A − 1)$ in the ground state is detected in coincidence with the scattered electron [3], has been shown to be very useful in clarifying the origin of the EMC effect and, at the same time, in providing valuable information on quark hadronization in the medium, complementary to the information obtained so far by the analysis of the classical SIDIS process. In Ref. [3], however, the plane-wave impulse approximation (PWIA) was assumed to be the basic mechanism of the process. A relevant step forward was made in Ref. [4], where the theoretical approach was extended by considering the final state interaction of the hadronizing debris (the leading quark and the diquark) with the nucleons of the nucleus $(A − 1)$. This was done within a theory of FSI based on the eikonal approximation with the debris-nucleon interaction cross sections calculated by the hadronization model of Ref. [5]. In Ref. [6] this theory of FSI was applied to the treatment of the process ^{2}H$(e, e'p)X$ in the limit of asymptotic values of Q^2, whereas in Ref. [7] finite values of Q^2 were considered.

In the present paper, the SIDIS processes ^{2}H$(e, e'p)X$ and ^{3}He$(e, e'd)X$ will be analyzed in detail, presenting in the former case a comparison with recent experimental data from the Thomas Jefferson National Accelerator Facility (JLab) [8,9]. Since accurate nuclear wave functions, corresponding to realistic nucleon-nucleon (*NN*) interactions, e.g., the Urbana AV18 interaction [10], can be used for both the two- and three-body nuclei, our calculations can serve as a reference guide for calculations in complex nuclei. In Sec. II the theoretical cross sections of the process $A(e, e'(A − 1))X$, both in PWIA and with consideration of FSI, will be discussed; in Sec. III, the SIDIS process ^{2}H$(e, e'p)X$ will be illustrated and a comparison between theoretical calculations and experimental data will be presented; in Sec. IV the process ^{3}He$(e, e'd)X$ is analyzed, illustrating how the SIDIS process we are considering could be used to tag the EMC effect and to investigate hadronization mechanisms.

_____
[*]On leave from Bogoliubov Lab. Theor. Phys., 141980, JINR, Dubna, Russia.

II. CROSS SECTION OF THE PROCESS $A(e, e'(A-1))X$ WITH ACCOUNT OF FSI

The Feynman diagrams corresponding to the PWIA and FSI cross sections are shown in Fig. 1. These diagrams describe the so-called spectator mechanism in which the virtual photon hits a quark of a nucleon of the target A, and the nucleus $(A-1)$ coherently recoils and is detected in coincidence with the scattering electron. It is clear that if the target nucleus is a deuteron, the recoiling nucleus, within the spectator mechanism, can only be a nucleon, which, however, can in principle arise from other mechanisms, e.g., current and/or target fragmentation. Target fragmentation has been analyzed in Ref. [7], whose conclusions will be briefly recalled in Sec. III; from now on, we will only consider the spectator mechanism. If, on the contrary, the target is a nucleus with $A > 2$, the detection of an $(A-1)$ nucleus not only is strong evidence of the correctness of the spectator mechanism, but also it can provide information on the nature of the FSI between the nucleon debris and $(A-1)$ nucleons. In PWIA the SIDIS differential cross section reads as follows [3,4,7]:

$$\sigma^{A,\text{PWIA}}\left(x_{Bj}, Q^2, |\boldsymbol{P}_{A-1}|, y_A, z_1^{(A)}\right)$$

$$\equiv \sigma^{A,\text{PWIA}} = \frac{d\sigma^{A,\text{PWIA}}}{dx_{Bj}\, dQ^2\, d\boldsymbol{P}_{A-1}}$$

$$= K^A\left(x_{Bj}, Q^2, y_A, z_1^{(A)}\right) z_1^{(A)}$$

$$\times F_2^{N/A}\left(x_A, Q^2, k_1^2\right) n_0^A(|\boldsymbol{P}_{A-1}|). \tag{1}$$

Here $Q^2 = -q^2 = -(k_e - k'_e)^2 = \boldsymbol{q}^2 - \nu^2 = 4E_e E'_e \sin^2\frac{\theta_e}{2}$ is the four-momentum transfer (with $\boldsymbol{q} = \boldsymbol{k}_e - \boldsymbol{k}_{e'}$, $\nu = E_e - E'_e$, and $\theta_e \equiv \theta_{\widehat{\boldsymbol{k}_e\boldsymbol{k}_{e'}}}$); $y = \nu/E_e$; $x_{Bj} = Q^2/2m_N\nu$ is the Bjorken scaling variable, with m_N denoting the nucleon mass; $k_1 \equiv (k_{10}, \boldsymbol{k}_1)$, with $\boldsymbol{k}_1 \equiv -\boldsymbol{P}_{A-1}$, is the four-momentum of the hit nucleon; $F_2^{N/A}$ is the DIS structure function of the nucleon N in the nucleus A, depending upon the nucleus scaling variable x_A and Q^2 [*cf.* Eq. (3)]; and eventually, $K^A(x_{Bj}, Q^2, y_A, z_1^{(A)})$ is the following kinematical factor (note that in Ref. [7] y^A, $z_1^{(A)}$, and K^A were denoted y_1, z_1, and K, respectively):

$$K^A\left(x_{Bj}, Q^2, y_A, z_1^{(A)}\right)$$

$$= \frac{4\alpha_{\text{em}}^2}{Q^4}\frac{\pi}{x_{Bj}}\left(\frac{y}{y_A}\right)^2\left[\frac{y_A^2}{2} + (1-y_A) - \frac{k_1^2 x_{Bj}^2 y_A^2}{z_1^{(A)2} Q^2}\right]. \tag{2}$$
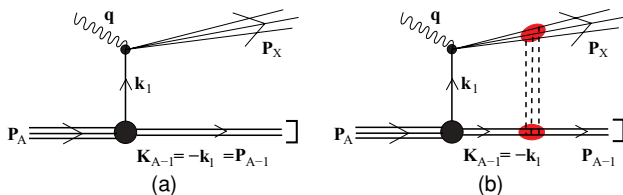

FIG. 1. (Color online) PWIA (a) and the FSI (b) contributions to the SIDIS process $A(e, e'(A-1))X$.

The A-dependent kinematical variables of the process are

$$y_A = \frac{k_1 q}{k_1 k_e}, \quad x_A = \frac{x_{Bj}}{z_1^{(A)}}, \quad z_1^{(A)} = \frac{k_1 q}{m_N \nu}, \tag{3}$$

In Eq. (2), α_{em} denotes the electromagnetic fine structure constant, and in Eq. (1) the angular dependence of $\boldsymbol{P}_{A-1}$ is provided by y_A and $z_1^{(A)}$. Note that since at high values of Q^2 one has $y \sim y_A$ (in the Bjorken limit $y = y_A$), the factor $(\frac{y}{y_A})^2$ in the cross section (1) is often omitted (see, e.g., Ref. [8]).

The relevant nuclear quantity in Eq. (1) is

$$n_0^A(|\boldsymbol{P}_{A-1}|) = \frac{1}{2J_A+1}\sum_{\mathcal{M}_A, \mathcal{M}_{A-1}}\left|\int d\mathbf{r}'_1 e^{i\mathbf{P}_{A-1}\mathbf{r}'_1}\right.$$

$$\left.\times\left\langle\Psi^0_{J_{A-1},\mathcal{M}_{A-1}}(\{\mathbf{r}'_i\})\Big|\Psi^0_{J_A,\mathcal{M}_A}(\mathbf{r}'_1,\{\mathbf{r}'_i\})\right\rangle\right|^2, \tag{4}$$

which represents the momentum distributions of the hit nucleon which was bound in the nucleus with minimum removal energy $E_{\text{min}} = |E_A| - |E_{A-1}|$, E_A and E_{A-1} being the ground-state energies of nuclei A and $(A-1)$, respectively. In Eq. (4) $\Psi^0_{J_A,\mathcal{M}_A}$ and $\Psi^0_{J_{A-1},\mathcal{M}_{A-1}}$ denote the intrinsic ground-state wave functions of nuclei A and $(A-1)$, respectively, $\mathbf{r}'_1$ describes the motion of the debris with respect to the center-of-mass (c.m.) of $(A-1)$, and, eventually, $\{\mathbf{r}'_i\}$ stands for a set of $A-2$ intrinsic variables. The nucleon momentum distributions generate nontrivial nuclear effects in SIDIS, whose nuclear dependence is also given by the quantities y_A and $z_1^{(A)}$, which differ from the corresponding quantities for a free nucleon ($y^N \equiv y = \nu/E_e$ and $z_1^{(N)} = 1$) if the off-mass shellness of the latter ($k_1^2 \neq m_N^2$) generated by nuclear binding is taken into account. Equation (1) is valid for finite values of Q^2, and for $A = 2$ it agrees with the expression used in Refs. [11–13]. Let us now consider the effects of the FSI. This is due to the propagation of the nucleon debris formed after γ^* absorption by a quark, followed by its hadronization, and by the hadronization of the diquark, and the interactions of the newly produced hadrons with the nucleons of $(A-1)$. Calculation of such a kind of FSI from first principle represents therefore a very complicated many-body problem, so that appropriate model approaches have to be developed. To this end, one is guided by the observation that in the kinematics we are considering (i) the momentum of the spectator nucleus $(A-1)$ is slow; (ii) the relative momentum between the debris (with momentum $\mathbf{p}_X$) and nucleon i of $(A-1)$ (with momentum $\mathbf{k}_i$), is very large, i.e., $|(\mathbf{p}_X - \mathbf{k}_i)| \simeq |\mathbf{q}| \gg |\mathbf{k}_i|$; and (iii) the momentum transfer in the interaction between the nucleon debris and $(A-1)$ is of the order typical for the scale of high-energy elastic NN scattering, i.e., much smaller than the incident momenta $\mathbf{p}_X$. As a consequence, most of the momentum carried by the virtual photon is transferred to the hit quark, and the exact rescattering wave function can be replaced by its eikonal approximation describing the propagation of the nucleon debris formed after γ^* absorption by a target quark, followed by hadronization processes and interactions of the newly produced hadrons with the spectator nucleons. The series of soft interactions between the produced hadrons and the spectator nucleons can be characterized by an effective cross section $\sigma_{\text{eff}}(z, Q^2, x_{Bj})$ depending upon

time (or the distance z traveled by the system X) [4]. The SIDIS cross section which includes FSI will therefore read as follows [4,6,7]:

$$\sigma^{A,\text{FSI}}\left(x_{Bj}, Q^2, |\boldsymbol{P}_{A-1}|, y_A, z_1^{(A)}\right)$$

$$\equiv \sigma^{A,\text{FSI}} = \frac{d\sigma^{A,\text{FSI}}}{dx_{Bj}\, dQ^2\, d\boldsymbol{P}_{A-1}} = K^A\left(x_{Bj}, Q^2, y_A, z_1^{(A)}\right)$$

$$\times z_1^{(A)} F_2^{N/A}\left(x_A, Q^2, k_1^2\right) n_0^{A,\text{FSI}}(\boldsymbol{P}_{A-1}), \qquad (5)$$

where $n_0^{A,\text{FSI}}(\boldsymbol{P}_{A-1})$ is the distorted momentum distribution of the bound nucleon

$$n_0^{A,\text{FSI}}(\boldsymbol{P}_{A-1})$$

$$= \frac{1}{2J_A + 1} \sum_{\mathcal{M}_A, \mathcal{M}_{A-1}} \left| \int d\mathbf{r}_1' e^{i\boldsymbol{P}_{A-1}\mathbf{r}_1'} \left\langle \Psi_{J_{A-1}, \mathcal{M}_{A-1}}^0(\{\mathbf{r}_i'\}) \right. \right.$$

$$\left. \left. \times \left| S_{\text{FSI}}^{XN}(\mathbf{r}_1, \ldots, \mathbf{r}_A) \right| \Psi_{J_A, \mathcal{M}_A}^0(\mathbf{r}_1', \{\mathbf{r}_i'\}) \right\rangle \right|^2. \qquad (6)$$

Here the quantity S_{FSI}^{XN} is the the debris-nucleon eikonal scattering S matrix

$$S_{\text{FSI}}^{XN}(\mathbf{r}_1, \ldots, \mathbf{r}_A) = \prod_{i=2}^{A} [1 - \theta(z_i - z_1)\Gamma(\mathbf{b}_1 - \mathbf{b}_i, z_1 - z_i)],$$

$$(7)$$

with the Q^2- and x_{Bj}-dependent profile function being

$$\Gamma^{XN}(\mathbf{b}_{1i}, z_{1i}) = \frac{(1 - i\,\alpha)\,\sigma_{\text{eff}}(z_{1i}, Q^2, x_{Bj})}{4\pi\, b_0^2} \exp\left[-\frac{\mathbf{b}_{1i}^2}{2\, b_0^2}\right],$$

$$(8)$$

where $\mathbf{r}_{1i} = \{\mathbf{b}_{1i}, \mathbf{z}_{1i}\}$, with $\mathbf{z}_{1i} = \mathbf{z}_1 - \mathbf{z}_i$ and $\mathbf{b}_{1i} = \mathbf{b}_1 - \mathbf{b}_i$. It can be seen that, unlike the standard Glauber eikonal approximation [14], the profile function Γ^{XN} depends not only upon the transverse relative separation but also upon the longitudinal separation $z_{1,i} = z_1 - z_i$ due to the z (or time) dependence of the effective cross section $\sigma_{\text{eff}}(z_{1i})$ and the θ function, $\theta(z_i - z_1)$. As already mentioned, the effective cross section $\sigma_{\text{eff}}(z_{1i})$ also depends on the total energy of the debris, $W_X^2 \equiv P_X^2$; if the energy is not high enough, the hadronization procedure can terminate inside the nucleus $(A - 1)$, after which the number of produced hadrons and the cross section $\sigma_{\text{eff}}(z_{1i}, x_{Bj}, Q^2) \equiv \sigma_{\text{eff}}(z)$ remain constant.

A. Effective debris-nucleon cross section

As already pointed out, although the profile function given by Eq. (8) resembles the usual Glauber form, it contains an important difference in that it depends also upon the longitudinal separation $z_{1i} = z_1 - z_i$ due to the z (or time) dependence of the effective cross section $\sigma_{\text{eff}}(z)$, which describes the interaction of the debris of the so-called active nucleon "1" with the spectator nucleon "i". The effective cross section $\sigma_{\text{eff}}(z)$ has been derived in detail in Ref. [4]. It has already been used in the description of SIDIS off nuclei in Refs. [6,7] and has been shown [15] to provide a good description of grey track production in muon-nucleus DIS at high energies [16]. Therefore, it only suffices to recall here that at the given point z, $\sigma_{\text{eff}}(z)$ consists of a sum of the nucleon-nucleon and pion-nucleon total cross sections, with the former describing the hadronization of the diquark into a nucleon and the latter increasing with z like the multiplicity of pions produced by the breaking of the color string and by gluon radiation, respectively, namely, $\sigma_{\text{eff}}(z)$ has the following form: $\sigma_{\text{eff}}(z) = \sigma_{\text{tot}}^{NN} + \sigma_{\text{tot}}^{\pi N}[n_M(z) + n_G(z)]$, where the Q^2- and x_{Bj}-dependent quantities $n_M(z)$ and $n_G(z)$ are the pion multiplicities due to the breaking of the color string and to gluon radiation; their explicit forms are given in Ref. [4]. Let us stress that hadronization is basically a QCD nonperturbative process, and, consequently, any experimental information on its effects on the SIDIS process we are considering would be a rather valuable one; since it has been shown in Ref. [6] that in the kinematical range where FSI effects are relevant the process is essentially governed by the hadronization cross section, this opens a new and important aspect of these reactions, namely, the possibility, through them, to investigate hadronization mechanisms by choosing a proper kinematics where FSI effects are maximized.

In Ref. [4] $\sigma_{\text{eff}}(z)$ was obtained in the limit of very high energies. In this paper, as in Ref. [7], we generalize the results of Ref. [4] to lower energies (e.g., JLab ones) by the following procedure. According to the hadronization model of Ref. [5], the process of pion production on a nucleon after γ^* absorption by a quark can schematically be represented as in Fig. 2: at the interaction point, a color string, denoted X_1, and a nucleon N_1, arising from target fragmentation, are formed; the color string propagates and gluon radiation begins. The first "pion" is created at $z_0 \simeq 0.6$ by the breaking
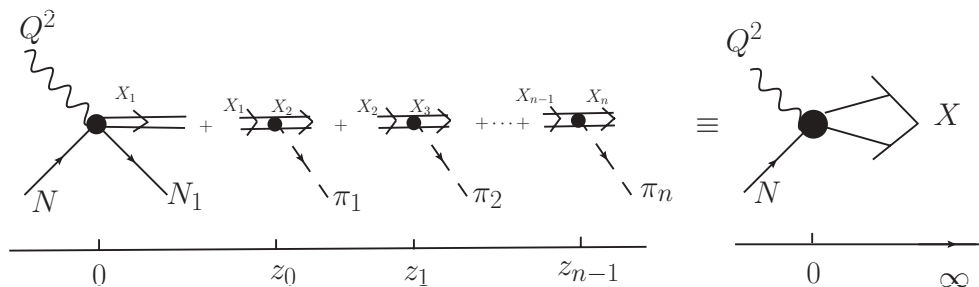

FIG. 2. Schematic representation of pion and nucleon N_1 production by quark and diquark hadronization leading to the FSI in the SIDIS process $A(e, e'(A - 1))X$.

of the color string, and pion production continues until it stops at a maximum value of $z = z_{max}$, when energy conservation does not allow further pions to be created, and the number of pions remains constant; we obtain

$$z_{max} = \frac{E_{loss}^{max}}{\kappa_{str} + \kappa_{gl}} = \xi \frac{E_X - E_{N_1}}{\kappa_{str} + \kappa_{gl}}, \qquad (9)$$

where (see Ref. [5]) $\kappa_{gl} = 2/(3\pi)\alpha_s(Q^2 - \lambda^2)$ (with $\lambda \approx 0.65$ GeV) and $\kappa_{str} = 0.2$ GeV^2 represent the energy loss ($\kappa = -dE/dz$) of the leading hadronizing quark due to the string breaking and gluon radiation, respectively; in Eq. (9) E_{loss}^{max} is the maximum energy loss, which can be expressed in terms of the energy of the nucleon debris E_X and the energy E_{N_1} of the nucleon created by target fragmentation at the interaction point. The maximum energy loss depends upon the kinematics of the process, and within the kinematics we have considered, it turns out that $\xi = 0.55$. It should be pointed out that once the total effective cross section $\sigma_{eff}(z)$ has been obtained, the elastic slope b_0 and the ratio α of the real to the imaginary parts of the elastic amplitude remain to be determined. This does not represent a problem at very high energies and for medium and heavy nuclei, as considered in Ref. [4], since in this case $\alpha \to 0$ and, within the optical limit, the cross section will only depend upon the convolution between the effective cross section $\sigma_{eff}(z' - z)$ and the nuclear density $\rho(\boldsymbol{b}, z')$, i.e., the quantity $S(\boldsymbol{b}, z) = \int dz' \, \rho(\boldsymbol{b}, z')\sigma_{eff}(z' - z)$. At lower energies, α and b_0 appear explicitly in the calculations. Their choice will be discussed in the next section.

III. PROCESS ^{2}H$(e, e'p)X$

A. Details of calculations

Within the spectator mechanism, γ^* interacts with a quark of the neutron, and the spectator proton recoils and is detected with momentum $\mathbf{P}_{A-1} \equiv \mathbf{p}_p$, with $\mathbf{p}_p = -\mathbf{k}_1$ in PWIA, and $\mathbf{p}_p \neq \mathbf{k}_1$ when FSI is considered (*cf.* Fig. 1) (note that the detected nucleon momentum $\mathbf{p}_p$ is denoted $\mathbf{p}_2$ in Ref. [7] and $\mathbf{p}_s$ in Refs. [8,9,11,13]). We calculated the process ^{2}H$(e, e'p)X$ at the kinematics of the recent JLab experiment [8,9] both in PWIA [Eq. (1)] and taking FSI into account [Eq. (5)]. We used deuteron wave functions generated by realistic NN potentials, in particular, the AV18 interaction [10]. For the nucleon deep-inelastic structure function F_2 we used the parametrization from Ref. [17] with the nucleon off-mass shell within the x-rescaling model, i.e., by using $x_A = x_{Bj}/z_1^{(A)}$, where $z_1^{(A)} = k_1 q/(m_p \nu)$ with $k_1^0 = M_D - \sqrt{m_p^2 + \mathbf{p}_p^2}$ (in what follows, all quantities, e.g., mass, momentum, cross section, etc., pertaining to ^{2}H will be labeled by a capital D). As for the quantities appearing in the profile function (8), we used the following procedure, which is appropriate for the kinematics we considered (see next section): σ_{eff} was calculated as explained in Sec. II with values $\sigma_{NN} = 40$ mb and $\sigma_{\pi N} = 30$ mb, and α and b_0 taken from world data on πN scattering, since the underlying FSI mechanism is described by the πN cross section and the pion multiplicities. The comparison of the results of our calculations, which contain no adjustable parameters, are presented in the next section and compared with available experimental data.

B. Comparison with experimental data and the effect of FSI

Experimental data on the process ^{2}H$(e, e'p)X$ were recently obtained at JLab [8,9] in the following kinematical regions: beam energy $E_e = 5.75$ GeV, four-momentum transfer $1.2 \lesssim Q^2 \lesssim 5.0$ (GeV/c)^2, recoiling proton momentum $0.28 \lesssim |\mathbf{p}_p| \leqslant 0.7$ GeV/c, proton emission angle $-0.8 \leqslant \cos\theta_{\mathbf{p}} \leqslant 0.7$ ($\theta_{\widehat{\mathbf{p} \cdot \mathbf{q}}} \equiv \theta_{\mathbf{p}}$), and invariant mass of the produced hadronic state $1.1 \leqslant W_X \leqslant 2.7$ GeV, with $W_X^2 = (k_1 + q)^2 = (P_D - p_p + q)^2$. The data have been plotted in terms of the reduced cross section

$$\sigma^{red}(x_{Bj}, Q^2, \mathbf{p}_p) = \frac{1}{K^A(x_{Bj}, Q^2, y_A, z_1^{(A)})} \left(\frac{y}{y_D}\right)^2 \\ \times \frac{d\sigma^{D,expt}}{dx_{Bj} dQ^2 d\mathbf{p}_p}, \qquad (10)$$

which, within our approach, would be

$$\sigma^{red}(x_{Bj}, Q^2, \mathbf{p}_p) \\ = \left(\frac{y}{y_D}\right)^2 z_1^{(D)} F_2^{N/D}(x_D, Q^2, k_1^2) n_0^{D,FSI}(\mathbf{p}_p), \qquad (11)$$

in agreement with the experimental definition of Ref. [8]. A comparison between theoretical calculations and the experimental data plotted vs $\cos\theta_{\mathbf{p}}$ at fixed values of Q^2, W_X, and $|\mathbf{p}_p|$, is presented in Fig. 3, which clearly shows that (i) apart from the very backward emission, the experimental data are dominated by the FSI; (ii) our model of FSI provides a satisfactory description of the experimental data in the backward direction and also around $\theta_{\mathbf{p}} \simeq 90°$ (a comparison of theoretical results and experimental data in the full range of kinematics of Ref. [8,9] will be presented elsewhere); and (iii) in the forward direction ($\theta_{\mathbf{p}} \lesssim 80°$), the spectator mechanism fails to reproduce the data, and it is clear that other production mechanisms are playing a role in this region.[1] For such a reason in what follows we will consider the region ($\theta_{\mathbf{p}} \gtrsim 80°$) where useful information on both the hadronization mechanism and the EMC effect can in principle be obtained, provided the data are analyzed in the proper way, getting rid of EMC effects, in the former case, and of nuclear effects, in the latter case. This problem will be clarified in the next section on the example of the process ^{3}He$(e, e'd)X$.

IV. PROCESS ^{3}He$(e, e'D)X$

A. Details of calculations

In the process ^{3}He$(e, e'd)X$, the virtual photon γ^* interacts with a quark of the proton, and the spectator deuteron recoils and is detected with momentum $\mathbf{P}_{A-1} \equiv \mathbf{P}_D$, with $\mathbf{P}_D = -\mathbf{k}_1$ in PWIA and $\mathbf{P}_D \neq \mathbf{k}_1$ when FSI is considered (*cf.* Fig. 1). We considered the process at kinematics similar to the ones of the 12-GeV upgraded JLab. Nuclear structure effects were taken care of within a full self-consistent and realistic

---

[1]An analysis of the JLab experimental data on the process $^2H(e, e'p)X$ recently appeared [21] after the completion of the present work.

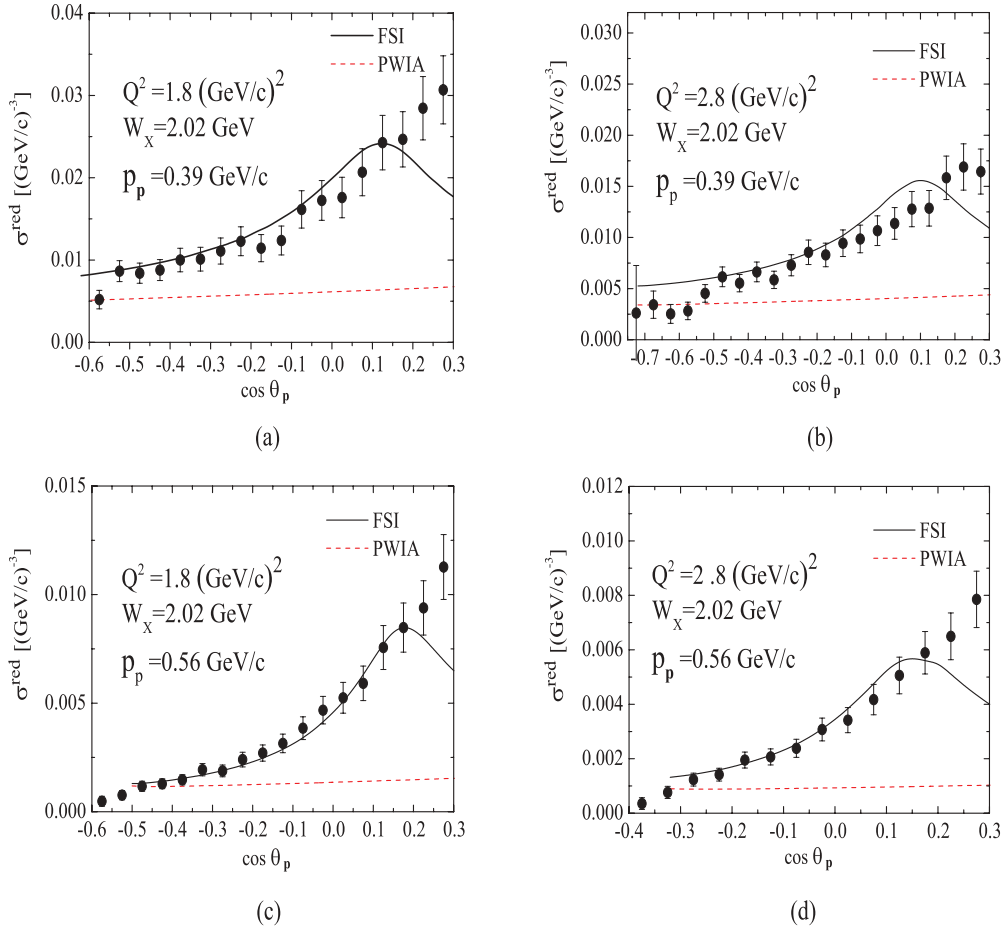FIG. 3. (Color online) Theoretical reduced cross section, Eq. (11), vs $\cos\theta_{\widehat{p\mathbf{q}}}$ ($\theta_{\widehat{p\mathbf{q}}} \equiv \theta_p$) compared with the experimental data of Refs. [8,9]. Each figure shows the reduced cross section calculated at fixed values of the four-momentum transfer Q^2, the invariant mass W_X of the hadronic state X, and the momentum $|\mathbf{p}_p| \equiv p_p$ of the detected proton. The error bars represent the sum in quadrature of statistical and systematic errors given in Refs. [8,9].

approach based upon the deuteron and ^{3}He wave functions obtained from an exact solution of the Schrödinger equation corresponding to the AV18 NN interaction; in particular, the three-nucleon wave functions correspond to those of Ref. [18]. For the nucleon structure function $F_2^{N/A}$ we used the parametrization from Ref. [17], with the nucleon off-mass shell within the x-rescaling model, i.e., $x_A = x_{Bj}/z_1^{(A)}$ where $z_1^{(A)} = k_1 q/(m_N \nu)$ with $k_1^0 = M_3 - \sqrt{M_D^2 + \mathbf{p}_D^2}$. Within such a framework, we demonstrate in the next sections how to tag the hadronization mechanism and the EMC effect, i.e., how to obtain information on (i) hadronization mechanisms, free from possible contaminations of unknown EMC effects, and (ii) the EMC effect, free from possible contamination of unknown nuclear structure effects.

B. Tagging the hadronization mechanisms

In Fig. 4 we show the cross section of the process ^{3}He$(e, e'd)X$ calculated by Eqs. (1) and (5) at two different values of the deuteron emission angle, corresponding to parallel ($\theta_{\widehat{P_D\mathbf{q}}} \equiv \theta_D = 180°$) and perpendicular ($\theta_{\widehat{P_D\mathbf{q}}} \equiv \theta_D = 90°$) kinematics, respectively. It can be seen that, as

in the case of the process ^{2}H$(e, e'p)X$, FSI increases with the momentum of the detected deuteron and is particularly relevant in perpendicular kinematics, which is the region one has to consider to obtain information about hadronization mechanisms. To this end, in order to minimize possible contaminations from the poor knowledge of the neutron structure function, the ratio of the cross sections for two different nuclei A and A' measured at the same value of x_{Bj} should be considered, since, within our approach one has

$$
\begin{aligned}
&R^{\text{expt}}\big(x_{Bj}, Q^2, |\boldsymbol{P}_{A-1}|, z_1^{(A)}, z_1^{(A')}, y_A, y_{A'}\big) \\
&= \frac{\sigma^{A,\text{expt}}\big(x_{Bj}, Q^2, |\boldsymbol{P}_{A-1}|, z_1^{(A)}, y_A\big)}{\sigma^{A',\text{expt}}\big(x_{Bj}, Q^2, |\boldsymbol{P}_{A-1}|, z_1^{(A')}, y_{A'}\big)} \\
&\rightarrow \frac{n_0^{(A,\text{FSI})}(\boldsymbol{P}_{A-1})}{n_0^{(A',\text{FSI})}(\boldsymbol{P}_{A-1})} \equiv R(A, A', \boldsymbol{P}_{A-1}), \quad (12)
\end{aligned}
$$

where the last step, as stressed in Ref. [3], is not valid exactly, for the factors $K(x_{Bj}, Q^2, y_A, z_1^{(A)})$ and $z_1^{(A)} F_2^{N/A}(x_D, Q^2, k_1^2)$ in Eq. (1) depend upon A via y_A and $z_1^{(A)}$. However, as discussed in detail in Ref. [3] [see Fig. 3 there and the discussion after Eq. (32)], at high values of Q^2 the factor
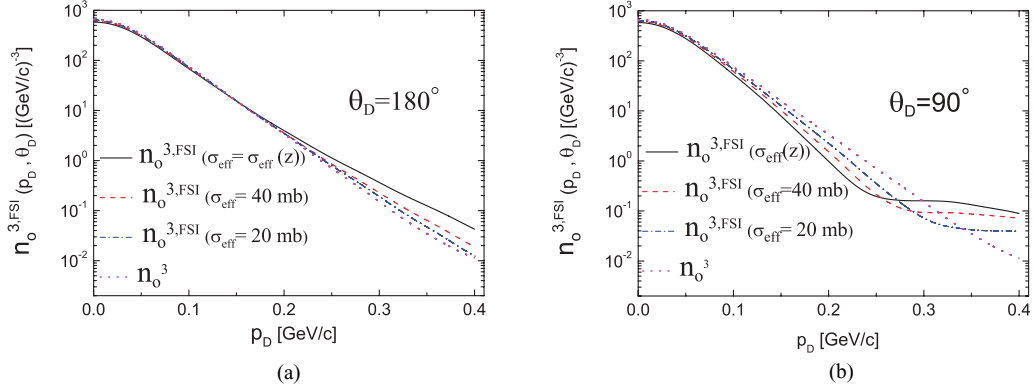
FIG. 4. (Color online) Distorted momentum distribution $n_0^{3,\text{FSI}}(\mathbf{P}_{A-1})$ [Eq. (6) with $\mathbf{P}_{A-1} \equiv \mathbf{p}_D$] in the process $^3\text{He}(e, e'd)X$ in parallel (a) and perpendicular (b) kinematics calculated with different effective debris-nucleon cross sections in Eq. (8): the effective debris-nucleon cross section $\sigma_{\text{eff}}(z) \equiv \sigma_{\text{eff}}(z, Q^2, x_{Bj})$ (full line) and two constant cross sections (dashed and dot-dashed lines). Also shown (dotted line) is the momentum distribution $n_0^3(|\mathbf{P}_{A-1}|)$ [Eq. (4)]. Calculations have been performed at the following kinematics: $E_e = 12$ GeV, $Q^2 = 6$ GeV$^2/c^2$, and $W_X^2 = 5.8$ GeV^2.

K^A differs only by a few percent from the free nucleon value K^N, i.e., becomes practically A independent ($K^A = K^N$ in the Bjorken limit); as for the A dependence of the ratio $z_1^{(A)} F_2^{N/A}/z_1^{(A')} F_2^{N/A'}$, it can be of the order of the EMC effect and in Ref. [3] has been numerically estimated to be at maximum of 5% (note that in the Bjorken limit and within a light cone approach, the ratio is exactly unity, being the nucleons on shell); at the same time, in the low nucleon momentum region we are considering, the momentum distributions of light nuclei may differ up to an order of magnitude (see Fig. 2 of Ref. [3]); it is clear therefore that the $|\mathbf{P}_{A-1}|$ dependence of the ratio (12) is governed by the ratio of the momentum distributions, and any reasonably expected A dependence of $F_2^{N/A}(x_A, Q^2, k_1^2)$ through x_A will not affect it.

The ratio for $A = 2$ and $A' = 3$ is shown in Fig. 5. It can be seen that at low values of the detected momentum, FSI plays only a minor role both in parallel and perpendicular kinematics.
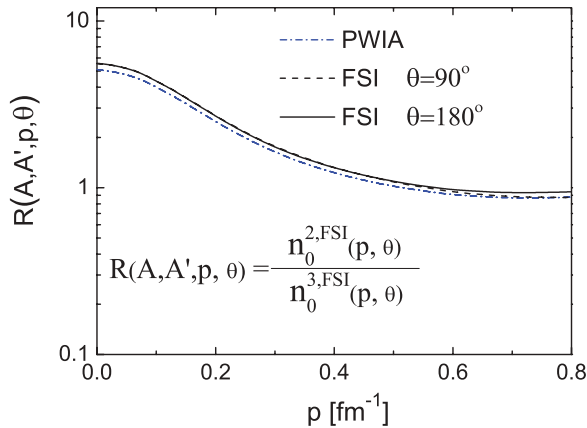

FIG. 5. (Color online) Ratio given by Eq. (12) with $A = {}^2\text{H}$ and $A' = {}^3\text{He}$, corresponding to the processes $^2\text{H}(e, e'p)X$ and $^3\text{H}(e, e'd)X$ in parallel ($\theta_p = \theta_D \equiv \theta = 180°$) and perpendicular ($\theta_p = \theta_D \equiv \theta = 90°$) kinematics, respectively. Protons and deuterons are detected with the same value of the momentum $|\mathbf{p}_p| = |\mathbf{p}_D| \equiv p$.

In this respect, we would like to stress once again that whereas the momentum dependence of the cross section is generated both by the momentum dependence of the distorted momentum distributions, and by a possible momentum dependence of the nucleon structure functions (see next section), the momentum dependence of the ratio (12) is only governed by the distorted momentum distribution; since the low momentum part of the momentum distribution is very well known for $A = 2$ and $A = 3$ systems (as well as for heavier nuclei), the experimental observation of a ratio similar to the one shown in Fig. 5, would provide strong evidence of the correctness of the spectator mechanism and of the FSI model; at the same time, the observation of strong deviations from the prediction shown in Fig. 5, would provide evidence of reaction mechanism and/or FSI effects which are missing in our model. Experiments on heavier nuclei, particularly at perpendicular kinematics and $|\mathbf{p}_{A-1}| \simeq 0.2$–0.4 GeV/$c$ (cf. Fig. 4), where the effects of FSI are expected to be more relevant [4], would be extremely useful in clarifying the mechanism of the FSI.

C. Tagging the EMC effect

To tag the EMC effect, i.e., if, how, and to what extent the nucleon structure function in the medium differs from the free structure function, one has to get rid of the effects due to the distorted nucleon momentum distributions and other nuclear structure effects; i.e., one has to consider a quantity which would depend only upon $F_2^{N/A}(x_A, Q^2, k_1^2)$. This can be achieved by considering the ratio of the cross sections on nucleus A measured at two different values of the Bjorken scaling variable x_{Bj} and x'_{Bj}, leaving unchanged all other quantities in the two cross sections, i.e., the ratio

$$
\begin{aligned}
R^{\text{expt}}&\left(x_{Bj}, x'_{Bj}, Q^2, |\mathbf{P}_{A-1}|, z_1^{(A)}, y_A\right) \\
&= \frac{\sigma^{A,\text{exp}}\left(x_{Bj}, Q^2, |\mathbf{P}_{A-1}|, z_1^{(A)}, y_A\right)}{\sigma^{A,\text{exp}}\left(x'_{Bj}, Q^2, |\mathbf{P}_{A-1}|, z_1^{(A)'}, y'_A\right)} \\
&\to \frac{F_2^{N/A}\left(x_A, Q^2, k_1^2\right)}{F_2^{N/A}\left(x'_A, Q^2, k_1^2\right)} \equiv R\left(x_{Bj}, x'_{Bj}, |\mathbf{P}_{A-1}|\right). \quad (13)
\end{aligned}
$$
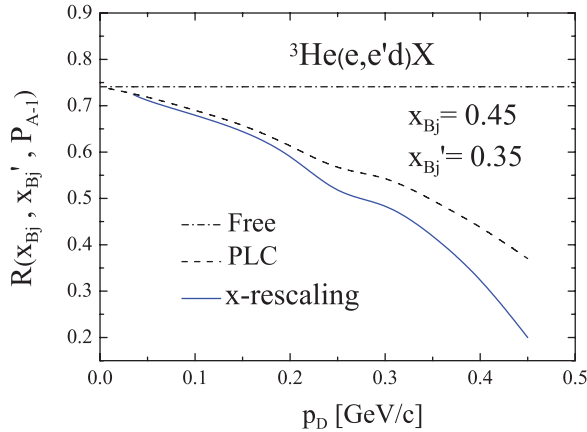
FIG. 6. (Color online) Ratio given by Eq. (13) corresponding to the process ^{3}He$(e, e'd)X$ calculated at two values of the Bjorken scaling variable x_{Bj} and with different nucleon structure functions. (i) Free structure function (dot-dashed line): $F_2^{N/A}(x^A) = F_2^{N/A}(x_{Bj})$; (ii) off mass-shell ($x$-rescaling) structure function (full line): $F_2^{N/A}(x^A) = F_2^{N/A}(x_{Bj}/z_1^A)$ with $z_1^A = k_1 q/(m_N \nu)$ and $k_1^0 = M_A - \sqrt{(M_{A-1}^*)^2 + \mathbf{P}_{A-1}^2}$; (iii) structure function with reduction of pointlike configurations (PLC) in the medium depending upon the nucleon virtuality $v(\mathbf{k}_1, E)$ [Eq. (15)] [19] (dashed line): $F_2^{N/A}(x^A) = F_2^N(x_{Bj}/z_1^N)\delta_A(x_{Bj}, v(\mathbf{k}_1, E))$ with $z_1^N = k_1 q/(m_N \nu)$ and $k_1^0 = M_A - \sqrt{m_N^2 + \mathbf{P}_{A-1}^2}$.

We considered the quantity (13) calculated in the following kinematical range: $2 \lesssim W_X^2 \lesssim 10$ GeV^2 and $Q^2 = 8$ (GeV/c)^2. At each value of W_X we changed $|\mathbf{P}_D|$ from zero to $|\mathbf{P}_D| = 0.5$ GeV/c, obtaining for different values of $|\mathbf{P}_D|$ different values of x_{Bj}. To minimize the effects of FSI, the angle $\theta_{\widehat{\mathbf{P}_D \cdot \mathbf{q}}}$ was chosen in the backward direction, $\theta_{\widehat{\mathbf{P}_D \cdot \mathbf{q}}} \sim 145°$ (*cf.* Fig. 4). Within such a kinematics, the effective cross section $\sigma_{\mathrm{eff}}(z_{1i}, x_{Bj}, Q^2)$ is the same for different values of W_X and, correspondingly, the distorted momentum distributions $n_0^{A,\mathrm{FSI}}$ will depend only upon $|\mathbf{P}_D|$ and cancel in the ratio (13). In this way, all nuclear structure effects, except possible effects of in-medium deformations of the nucleon structure function $F_2^{N/A}$, are eliminated, and one is left with a ratio which depends only upon the nucleon structure function $F_2^{N/A}$. Calculations have been performed using three different structure functions $F_2^{N/A}(x_A, Q^2, k_1^2)$:

(1) The free nucleon structure function from Ref. [17], exhibiting no EMC effects.

(2) The nucleon structure function pertaining to the x-rescaling model with the nucleon off-mass shell, i.e., $F_2^{N/A}(x_A, Q^2, k_1^2) \rightarrow F_2^N(x_A, Q^2) = F_2^N(\frac{x_{Bj}}{z_1^A}, Q^2)$, where $z_1^A = k_1 q/(m_p \nu)$ with $k_1^0 = M_A - \sqrt{M_{A-1}^{*2} + \mathbf{k}_1^2}$.

(3) The structure function from Ref. [19], which assumes that the reduction of the nucleon pointlike configurations (PLC) in the medium (see Ref. [11]) depends upon the nucleon virtuality

$$F_2^{N/A}(x_A, Q^2, k_1^2) \rightarrow F_2^{N/A}(x_{Bj}/z_1^N, Q^2)$$
$$\times \delta_A(x_{Bj}, v(|\mathbf{k}_1|, E)), \quad (14)$$

where $z_1^N = (m_N + |\mathbf{P}_D| \cos \theta_D)/m_N$. Here the reduction of the PLC is given by the quantity $\delta_A(x_{Bj}, v(\mathbf{k}, E))$, which depends upon the nucleon virtuality (see Ref. [19]):

$$v(|\mathbf{k}_1|, E) = \left(M_A - \sqrt{(M_A - m_N + E)^2 + \mathbf{k}_1^2} \right)^2 - \mathbf{k}_1^2 - m_N^2. \quad (15)$$

It should be stressed that the two medium-dependent structure functions provide similar results for the inclusive cross section and that our aim is to answer the question as to whether the SIDIS experiment we are proposing could discriminate between the two models. The results of calculations corresponding to the kinematics $E_e = 12$ GeV, $Q^2 = 8$ (GeV/c)^2, $\theta_D = 145°$, $x_{Bj} = 0.45$, $x'_{Bj} = 0.35$ are presented in Fig. 6. It can be seen that the discrimination between different models of the virtuality dependence of $F_2^{N/A}(x_A, Q^2, k_1^2)$ can indeed be achieved by a measurement of the ratio (13); as a matter of fact, at $|\mathbf{P}_D| \simeq 0.4$ GeV/c, the two structure functions differ by about 40%.

V. SUMMARY AND CONCLUSIONS

In this paper we considered the SIDIS process $A(e, e'(A - 1))X$ on complex nuclei proposed in Ref. [3] within the spectator model and the PWIA, and extended in Ref. [4] by the inclusion of the FSI between the hadronizing debris and the nucleons of the detected nucleus $(A - 1)$. We focused on ^{2}H and ^{3}He targets and extended the treatment of FSI, by considering it not only at very high energies, as originally done in Ref. [4], but also at lower energies like the ones of JLab. The reason for considering ^{2}H and ^{3}He is twofold: (i) nuclear effects can accurately be calculated, since realistic wave functions resulting from the exact solution of the Schrödinger equation can be used, and (ii) experimental data for deuteron targets have recently been obtained [8].

The results of our calculations for the process ^{2}H$(e, e'p)X$ show that the experimental data can be well reproduced in the kinematics when the proton is emitted mainly backward in the range $70° \lesssim \theta_p \lesssim 145°$, with the effects of FSI interaction being very small in the very backward direction and dominating the cross section around $\theta_p \simeq 90°$. It is very gratifying to see that the experimental data can be reproduced in a wide kinematical region, which make us confident of the correctness of the spectator model and the treatment of the FSI between the hadron debris and the detected proton.

At emission angles $\theta_p \lesssim 80°$, the number of detected protons is much higher than our predictions, which is clear evidence of the presence of production mechanisms different from the spectator one. Among possible mechanisms leading to forward proton production, target and/or current fragmentation should be the first processes to be taken into account. The first one has been analyzed in Ref. [7], finding that it contributes only forward and at proton momenta much higher than the ones typical of the JLab kinematics we have considered. The contribution from current fragmentation effects is under investigation.

It is clear that the SIDIS process on heavier nuclei, with detection of a complex nucleus $(A - 1)$ (e.g., ^{2}H, ^{3}He, etc.)

would be extremely useful, since the only mechanism for producing a recoiling $(A-1)$ nucleus would be the spectator mechanism. These experiments would be very useful in clarifying the origin of the discrepancy between theory and experiment we found in the forward hemisphere in the process ^{2}H$(e, e'p)X$. Also, as stressed in Ref. [4], they would be very useful in studying the early stage of hadronization at short formation times without being affected by cascading processes, unlike the DIS inclusive hadron production $A(e, e'h)X$ where most hadrons with small momentum originate from cascading of more energetic particles.

We have illustrated how by measuring the reduced cross section on two different nuclei at the same value of the detected momentum, the validity of the spectator mechanism and information on the survival probabilities of the spectator nuclei, i.e., on the hadronization mechanism, could be obtained; moreover, by measuring the cross section on the same nucleus, but at two different values of x_{Bj}, the EMC effect could be tagged. Experiments of the type we have discussed, e.g., ^{2}H$(e, e'p)X$, ^{3}He$(e, e'd)X$, ^{4}He$(e, e'$ ^{3}H$)X$, and ^{4}He$(e, e'$ ^{3}He$)X$, would be extremely useful, and it is gratifying to see that such experiments are being planned thanks to the development of proper recoil detectors [20]. We

would like to mention that we performed our calculations at the upgraded JLab kinematics, but, as suggested in Ref. [3], the SIDIS process we are proposing could in principle be investigated at an electron-ion collider, where higher values of Q^2 and a wider interval of x_{Bj} could be reached, which would make the basic assumption of the spectator model, *viz.,* the factorization assumption, even more reliable. The analysis of relevant kinematics and cross sections are underway and will be reported elsewhere.

[1] P. R. Norton, Rep. Prog. Phys. **66**, 1253 (2003).

[2] A. Accardi, F. Arleo, W. K. Brooks, D. D'Enterria, and V. Muccifora, Riv. Nuovo Cimento Soc. Ital. Fis. **032**, 439 (2010).

[3] C. Ciofi degli Atti, L. P. Kaptari, and S. Scopetta, Eur. Phys. J. A **5**, 191 (1999).

[4] C. Ciofi degli Atti and B. Kopeliovich, Eur. Phys. J. A **17**, 133 (2003).

[5] B. Z. Kopeliovich, J. Nemchik, E. Predazzi, and A. Hayashigaki, Eur. Phys. J. A **19S1**, 111 (2004).

[6] C. Ciofi degli Atti , L. P. Kaptari, and B. Z. Kopeliovich, Eur. Phys. J. A **19**, 145 (2004).

[7] V. Palli, C. Ciofi degli Atti, L. P. Kaptari, C. B. Mezzetti, and M. Alvioli, Phys. Rev. C **80**, 054610 (2009).

[8] A. V. Klimenko *et al.*, Phys. Rev. C **73**, 035212 (2006).

[9] S. E. Kuhn (private communication).

[10] R. B. Wiringa, V. G. J. Stoks, and R. Schiavilla, Phys. Rev. C **51**, 38 (1995).

[11] L. L. Frankfurt and M. I. Strikman, Phys. Rep. **160**, 235 (1988).

[12] W. Melnitchouk, M. Sargsian, and M. I. Strikiman, Z. Phys. A **359**, 99 (1997).

[13] S. Simula, Phys. Lett. B **387**, 245 (1996).

[14] R. J. Glauber, in *Lectures in Theoretical Physics*, edited by W. E. Brittin *et al.* (Interscience, New York, 1959), Vol. 1, p. 315.

[15] C. Ciofi degli Atti and B. Kopeliovich, Phys. Lett. B **606**, 281 (2005).

[16] M. R. Adams *et al.* (E665 Collaboration), Z. Phys. C **65**, 225 (1995).

[17] B. Adeva *et al.* (SM Collaboration), Phys. Lett. B **412**, 414 (1997).

[18] A. Kievsky, S. Rosati, and M. Viviani, Phys. Rev. Lett. **82**, 3759 (1999); A. Kievsky (private communication).

[19] C. Ciofi degli Atti, L. L. Frankfurt, L. P. Kaptari, and M. I. Strikman, Phys. Rev. C **76**, 055206 (2007).

[20] See, e.g., Nuclear Exclusive and Semi-inclusive Physics with a New CLAS12 Low Energy Recoil Detector, a Letter of Intent to the Jefferson Lab PAC, K. Hafidi *et al.*, spokespersons, and private communication.

[21] W. Cosyn and M. Sargsian, arXiv:1012.0293v2 [nucl-th].